Biochemical Pharmacology 203 (2022) 115184

Contents lists available at ScienceDirect

Biochemical Pharmacology

journal homepage: www.elsevier.com/locate/biochempharm

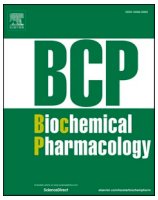

Enhanced cytotoxicity of a novel family of ATPase inhibitors in colorectal cancer cells with high NAT2 activity

Xiaonan Zhang [a], Ece Akcan [a], Mario Correia [b], Natallia Rameika [a], Snehangshu Kundu [a], Ivaylo Stoimenov [a], Veronica Rendo [a,c], Anna U. Eriksson [d], Martin Haraldsson [e], Daniel Globisch [b], Tobias Sjöblom [a,*]

[a] Department of Immunology, Genetics and Pathology, Uppsala University, SE-751 85 Uppsala, Sweden
[b] Department of Chemistry, BMC, Science for Life Laboratory, Uppsala University, SE-751 24 Uppsala, Sweden
[c] Department of Cancer Biology, Dana Farber Cancer Institute, Boston, MA, 02215, USA
[d] Department of Chemistry, CBCS, KBC-C4, Umeå University, SE-901 87 UMEÅ, Sweden
[e] Chemical Biology Consortium Sweden (CBCS), Science for Life Laboratory, Department of Medical Biochemistry and Biophysics, Karolinska Institutet, Stockholm, Sweden

ARTICLE INFO

Keywords:
Loss of heterozygosity (LOH)
ATPase inhibitors
Arylamine *N* acetyltransferase 2 (NAT2)
Nf-kB pathway
Small molecule therapeutics
Colorectal cancer

ABSTRACT

Loss of heterozygosity (LOH) is a hallmark feature of cancer genomes that reduces allelic variation, thereby creating tumor specific vulnerabilities which could be exploited for therapeutic purposes. We previously reported that loss of drug metabolic arylamine *N*-acetyltransferase 2 (NAT2) activity following LOH at 8p22 could be targeted for collateral lethality anticancer therapy in colorectal cancer (CRC). Here, we report a novel compound CBK034026C that exhibits specific toxicity towards CRC cells with high NAT2 activity. Connectivity Map analysis revealed that CBK034026C elicited a response pattern related to ATPase inhibitors. Similar to ouabain, a potent inhibitor of the Na^+/K^+-ATPase, CBK034026C activated the Nf-kB pathway. Further metabolomic profiling revealed downregulation of pathways associated with antioxidant defense and mitochondrial metabolism in CRC cells with high NAT2 activity, thereby weakening the protective response to oxidative stress induced by CBK034026C. The identification of a small molecule targeting metabolic vulnerabilities caused by NAT2 activity provides novel avenues for development of anticancer agents.

1. Introduction

Colorectal cancer (CRC) ranks third in incidence but second in mortality with nearly 2 million incident cases and 935,000 deaths in 2020 [1]. Surgery followed by chemotherapy or radiotherapy is the mainstay of CRC treatment and several targeted therapies for incurable metastatic CRCs have been developed [2]. However, therapy resistance eventually emerges [3]. One challenge is the lack of efficient agents which specifically kill tumor cells while sparing normal tissues. It was expected that cancer genome sequencing would unravel novel actionable targets [4–6]. However, these efforts uncovered few oncogene targets but revealed that the cancer genome landscape was dominated by tumor suppressor genes [7]. Additionally, most frequently mutated oncogenes have proven to be challenging targets for cancer therapy [8–10]. Innovative concepts to specifically target CRC tumor cells are therefore urgently needed.

Several strategies seeking to target somatic loss of bystander genes which are near tumor suppressor genes have recently been developed [11–14]. Loss of heterozygosity (LOH), a consequence of several different types of structural mutations in cancer genomes, is observed in >90% of human cancers, and can lead to loss of tumor suppressor gene function. Another consequence of LOH is heterozygous loci permanently losing one of their two parental alleles, thus reducing genetic variation in the tumor genome [7,15,16]. In certain types of cancers, such as CRC, LOH can affect more than 20% of the genome [15], causing loss of allelic variation in thousands of genes. Together, LOH events lead to genetic

Abbreviations: APA, 6-(4-aminophenyl)-*N*-(3,4,5-trimethoxyphenyl) pyrazin-2-amine; BSO, L-Buthionine sulphoximine; CRC, Colorectal cancer; GSTs, Glutathione *S*-transferases; HMOX-1, Heme oxygenase-1; LOH, Loss of heterozygosity; NAT2, Arylamine *N*-acetyltransferase 2; ROS, Reactive oxygen species; SNVs, Single nucleotide variants.

* Corresponding author.
E-mail address: tobias.sjoblom@igp.uu.se (T. Sjöblom).

https://doi.org/10.1016/j.bcp.2022.115184
Received 24 May 2022; Received in revised form 15 July 2022; Accepted 18 July 2022
Available online 22 July 2022

differences between tumor and normal cells, creating potential vulnerabilities which could be further targeted by low molecular weight drugs or other means.

We previously reported that recurring LOH at the *NAT2* locus on 8p22 in CRC could be exploited for anticancer therapy [17]. The *NAT2* gene is highly polymorphic and has more than 100 known single nucleotide variants (SNVs) in the protein coding sequence [18]. Arylamine *N*-acetyltransferase 2 (NAT2) is a cytosolic xenobiotic metabolizing enzyme with an essential role in the detoxification and metabolism of many drugs and carcinogens [19]. The detoxification and drug metabolism process requires different phaseI and phaseII enzymes that increase the hydrophilicity of these xenobiotics [20]. *NAT2* plays an essential role in the phaseII clearance of aromatic amines, hydrazines, and hydroxylamines by delivering an acetyl group from acetyl coenzymeA [21] (Figure1A). The expression of NAT2 is highest in the liver, followed by the small intestine and colon [22]. The highly polymorphic SNVs of *NAT2* alleles allows for the classification of individuals into rapid, intermediate, or slow acetylators [23]. Seven common single nucleotide polymorphisms (SNPs) define the different *NAT2* allele groups. *NAT2*4* is the wild-type allele. *NAT2*4*, *NAT2*11*, *NAT2*12*, and *NAT2*13* encode enzyme variants with rapid acetylator phenotype. *NAT2*5*, *NAT2*6*, *NAT2*7* and *NAT2*14* encode enzyme variants with slow acetylator phenotype [24]. Intermediate acetylators harbor one copy of a rapid and one copy of a slow acetylator allele ($NAT2^{slow/rapid}$). During the early development of CRC, a heterozygous patient ($NAT2^{slow/rapid}$) may lose the $NAT2^{rapid}$ allele by LOH, effectively rendering the tumor with >10-fold less NAT2 activity [25]. We previously established cell models expressing the rapid *NAT2*13A* or the slow *NAT2*6A* (rs1799930) acetylator allele and identified a cytotoxic low molecular weight compound APA (6-(4-aminophenyl)-*N*-(3,4,5-trimethoxyphenyl) pyrazin-2-amine) selectively killing CRC cells harboring only the slow *NAT2*6* allele by screening a selected set of 176 compounds from a total library size of 189,018 [17]. To our knowledge, this was the first proof of feasibility of targeting loss of non-disease-causing variant alleles of a non-essential enzyme to inhibit cancer cell growth. Here, we have performed a cell-based screen of chemical diversity to identify agents whose toxicity is modulated by cellular NAT2 activity. From ~33 K screened compounds we discovered and characterized CBK034026C, which elicited a response pattern related to ATPase inhibitors and preferentially killed cancer cells expressing rapid NAT2.

2. Results

2.1. Identification of agents with NAT2 activity dependent cytotoxicity through chemical library screening

We previously established CRC cell models expressing the prevalent rapid *NAT2*13A* ($NAT2^{rapid}$) or slow *NAT2*6A* (rs1799930, $NAT2^{slow}$) alleles and identified a cytotoxic low molecular weight compound, APA, selectively killing CRC cells with slow NAT2 activity [17]. Here, to identify novel drugs targeting the differential activity of NAT2 that arises in CRC cells through LOH or copy number alterations during tumor development, we performed a cell-based screen of 33,000 compounds available at the Chemical Biology Consortium Sweden (CBCS) (Fig. 1B). The average plate Z'-factor was 0.76–0.84, and the previously identified APA compound was re-discovered, confirming the robustness of the procedure. In this screen, we used selection criteria described in Fig. 1C, 3 compounds exhibiting preferential toxicity to $NAT2^{slow}$ CRC cells (CBK269664, CBK003557 and CBK062835, Fig. 1D) and 5 with preferential toxicity to $NAT2^{rapid}$ cells (CBK034026C, CBK008822, CBK263551, CBK018566 and CBK267247) were identified (Fig. 1E). As the $NAT2^{slow}$ selective compounds showed low toxicity and $IC_{50} > 50$ μM (Fig. 1F), they were not selected for further characterization. On the other hand, CBK034026C, CBK008822, CBK263551, CBK018566 and CBK267247 displayed higher potency with a ≥ 3-fold difference in IC_{50} in $NAT2^{rapid}$ versus $NAT2^{slow}$ cells (Fig. 1G). To make sure that the observed differences were dependent on NAT2 activity rather than the genetic background, we evaluated CBK034026C, CBK008822, CBK263551, CBK018566 and CBK267247 on DLD-1 $NAT2^{rapid}$ versus $NAT2^{slow}$ cells. A consistent pattern of preferential killing of $NAT2^{rapid}$ cells was observed for CBK034026C (Fig. 1H), supporting that the effect was dependent on NAT2 activity [17]. Taken together, we decided to focus our attention on CBK034026C as this compound had a significant difference in measured IC_{50} between $NAT2^{rapid}$ ($IC_{50} = 2.43$ μM) versus $NAT2^{slow}$ ($IC_{50} = 11.14$ μM) cells and a difference in IC_{50} was observed in two different genetic backgrounds.

2.2. CBK034026C and analogues display NAT2 activity dependent cytotoxicity

To better understand the NAT2 activity dependent toxicity of CBK034026C, we sought to identify structural analogues with a similar response pattern to CBK034026C. Through a structure-based search, 10 analogues were found and first tested in RKO cell models. Similar to CBK034026C, CBK034296T, CBK036384T, CBK038119 and CBK029030C show a consistent pattern of preferential killing of $NAT2^{rapid}$ cells, but only CBK034296T, CBK036384T and CBK038119 displayed the same response pattern in DLD-1 cell models (Fig. 2A and 2B). CBK034026C, CBK034296T, CBK036384T and CBK038119 share the same core structure, but different R1 and R2 groups (Fig. 2C and 2D). NAT2 is a cytosolic enzyme with a specific role in the metabolism of many drugs [19]. We therefore sought to determine whether CBK034026C was a direct NAT2 enzyme substrate. We incubated CBK034026C with recombinant human NAT2 protein and measured the acetylation products using mass spectrometry-based metabolomics [26]. Whereas an acetylation product was observed for APA, no acetylation products were detected for CBK034026C (Fig. 2E), demonstrating that CBK034026C is not a direct NAT2 substrate. We as well checked other screen hits using the RKO cell models. None of them (CBK008822, CBK263551, CBK018566 or CBK267247) were NAT2 substrates (Fig. 2F). We then asked whether CBK034026C is an inhibitor of NAT2 by incubating recombinant NAT2 protein with increasing concentrations of CBK034026C along with a known NAT2 substrate (APA). As the APA acetylation product was detected only in presence of recombinant NAT2 and regardless of the concentration of CBK034026C, we could refute that CBK034026C is a NAT2 inhibitor (Fig. 2G). Thus, the cytotoxicity of CBK034026C is most likely exerted through other cellular systems whose activity or function are influenced by NAT2.

2.3. Compound CBK034026C and its analogue CBK034296T elicit similar cellular effects as the Na^+/K^+-ATPase inhibitors

To decipher the differential effect of CBK034026C on cell growth in $NAT2^{rapid}$ and $NAT2^{slow}$ cells, we performed a Connectivity Map analysis (C-MAP), whereby genes, drugs, and disease states are translated into common gene-expression signatures to systematically define the cellular effects of a given compound with unknown target or mechanism of action [27]. Gene set enrichment analysis of the L1000 gene expression data revealed that CBK034026C and its analogue CBK034296T had highest similarity to the pharmacologic class of ATPase (Adenosine 5′-TriPhosphatase) inhibitors (Fig. 3A and 3B). The ATPases constitute a group of enzymes that catalyze hydrolysis of a phosphate bond in adenosine triphosphate (ATP) to form adenosine diphosphate (ADP), have essential roles in energy conservation, active transport and pH homeostasis in all known forms of life [28,29]. Based on the difference in structure and the type of ion that they transport, ATPases are divided in three major classes: F-ATPases (e.g. mitochondrial H^+-ATPase), P-ATPases (e.g. $Ca2^+$-ATPase, Na^+/K^+-ATPase) and V-ATPases (e.g. lysosomal H^+-ATPase) [30]. To determine which category of ATPases that CBK034026C and its analogue CBK034296T inhibit, we examined the top 10 ranked compounds belonging to the perturbagens of ATPase inhibitors (Fig. 3C). Interestingly, except the last compound oligomycin-

A

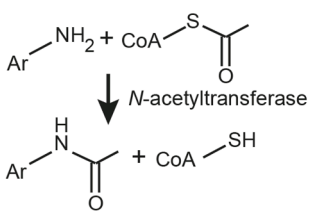

B

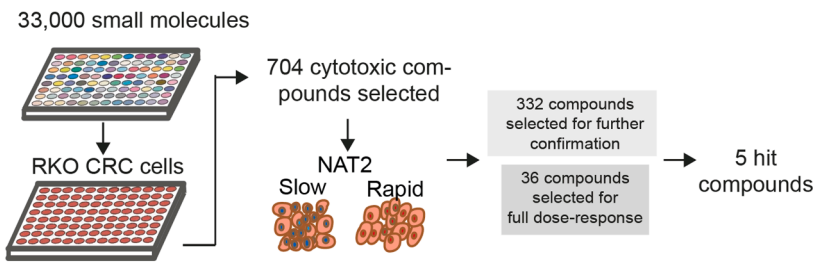

C

Table 1: Hit selection criteria

1 Reject all with viability >80% of DMSO in both cell-lines at 10 μM concentration
2 Select all with viability <50% of DMSO in both cell-lines at 1.25 μM concentration
3 Select all with % viability NAT2 rapid activity/% viability NAT2 slow activity at 10 μM >1.2
4 Select all with % viability NAT2 rapid activity/% viability NAT2 slow activity at 5 μM >1.2
5 Select all with % viability NAT2 rapid activity/% viability NAT2 slow activity at 1.25 μM >1.2
6 Select all with % viability NAT2 rapid activity/% viability NAT2 slow activity at 10 μM <0.6
7 Select all with % viability NAT2 rapid activity/% viability NAT2 slow activity at 5 μM <0.6
8 Select all with % viability NAT2 rapid activity/% viability NAT2 slow activity at 1.25 μM <0.6

D

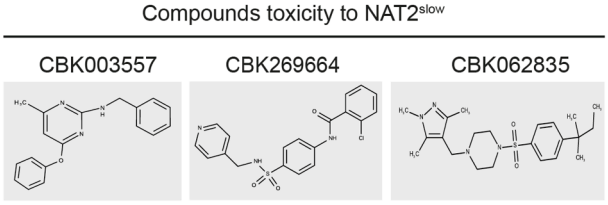

F

IC_{50} in RKO cells

Compound ID	NAT2 rapid (μM)	NAT2 slow (μM)
APA	2.53	0.85
CBK003557	81.47	73.82
CBK269664	>50	~50
CBK062835	107.5	52.81

G

IC_{50} in RKO cells

Compound ID	NAT2 rapid (μM)	NAT2 slow (μM)	Ratio (slow/rapid)
APA	2.53	0.85	0.33
CBK034026C	2.43	11.14	4.58
CBK008822	3.60	16.36	4.54
CBK263551	0.42	6.14	14.62
CBK018566	3.22	9.17	2.85
CBK267247	0.78	2.27	2.91

E

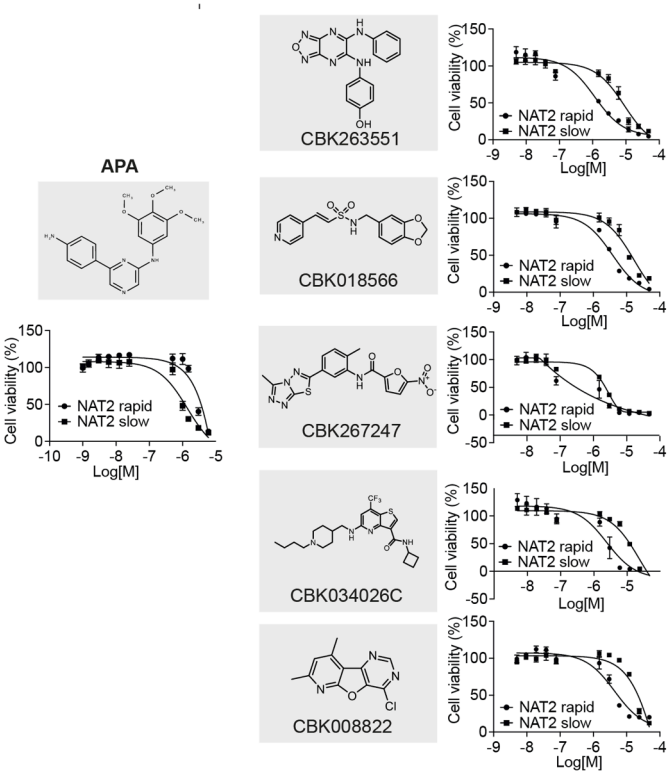

H

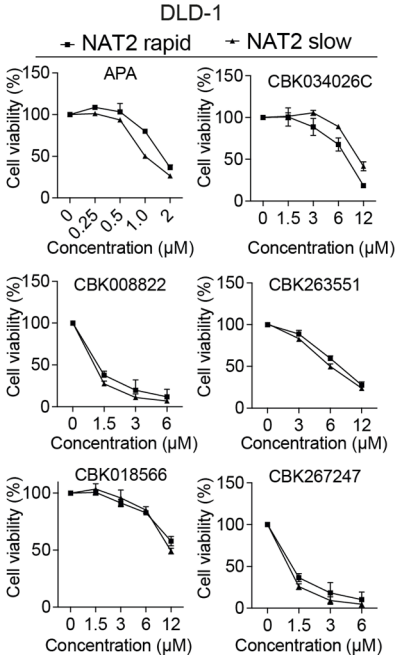

(caption on next page)

Fig. 1. Identification of agents with NAT2 activity dependent cytotoxicity through primary chemical library screening A. Enzyme reaction catalyzed by arylamine *N*-acetyltransferase 2 (NAT2). B. Workflow of the cell-based drug screen. A total of ~33,000 compounds were assessed in a cell-based screen in 384-well plates to find compounds that exhibited selective toxicity to either $NAT2^{rapid}$ or $NAT2^{slow}$ cells. C. Hit selection criteria used in the 33 K compounds library screening. D. Three compounds (CBK269664, CBK003557 and CBK062835) exhibiting greater toxicity to $NAT2^{slow}$. E. Five hits (CBK034026C, CBK008822, CBK263551, CBK018566 and CBK267247) selectively killing $NAT2^{rapid}$ cells were identified along with a known compound (APA) selectively killing $NAT2^{slow}$ cells. F. Three compounds (CBK269664, CBK003557 and CBK062835) exhibiting greater toxicity to $NAT2^{slow}$ show $IC_{50} > 50$ μM in both RKO $NAT2^{rapid}$ and $NAT2^{slow}$ cells. G. The IC_{50} values of the discovered hit compounds exhibiting greater toxicity to $NAT2^{rapid\ cells}$. H. A consistent pattern of preferential killing of DLD-1 $NAT2^{rapid}$ cells was observed for CBK034026C. The data are expressed as the mean ± SD of three independent experiments.

a, described as a F0F1 H^+ -ATPase inhibitor [31], which had enrichment score <90, the other 9 compounds including digitoxin, digoxin [32] and ouabain [33] are known inhibitors of Na^+/K^+-ATPase, indicating that CBK034026C and its analogue CBK034296T targeted the activity of Na^+/K^+-ATPase. To confirm this finding, we tested CBK034026C along with ouabain in an ATPase enzyme activity assay. Significant inhibition of ATPase activity was observed in both RKO and DLD-1 cells treated with CBK034026C (Fig. 3D). Moreover, consistent with the observation from CBK034026C, the ATPase inhibitors digitoxin and ouabain also exhibited stronger toxicity to $NAT2^{rapid}$ cells (Fig. 3E and 3F), supporting the finding that CBK034026C is an Na^+/K^+-ATPase inhibitor.

2.4. Reprogramming of mitochondrial metabolism by NAT2

For mechanistic understanding of the NAT2 dependent toxicity of CBK034026C and analogues, we next assessed the metabolic differences between CRC cells with rapid or slow NAT2 alleles using mass spectrometry-based metabolomics [26]. Interestingly, the metabolic pathways of aspartate and asparagine, glutamate and glutathione metabolism were significantly upregulated in $NAT2^{slow}$ cells compared to $NAT2^{rapid}$ cells (Fig. 4A). Since all the top three metabolic pathways are critical in maintaining functional mitochondria (Fig. 4B), we hypothesized that altered activity of NAT2 might lead to reprograming of mitochondrial metabolism. Interestingly, we observed an accumulation of glutathione in $NAT2^{slow}$ cells (Fig. 4C). Glutathione is an indispensable component of the antioxidant defense systems [34,35]. An upregulation of glutathione metabolism can lead to increased antioxidant capacity, and vice versa. Indeed, when $NAT2^{rapid}$ and $NAT2^{slow}$ cells were treated with increasing concentrations of L-Buthionine sulphoximine (BSO), an inhibitor of GSH synthesis, almost no cell death was observed in $NAT2^{slow}$ cells even at the highest concentration of 100 mM BSO, whereas ~20% cell death was noticed at 0.1 mM and ~50% at 10 mM in $NAT2^{rapid}$ cells (Fig. 4D). We therefore hypothesized that differential antioxidant capacity could be relevant to the NAT2 dependent response to CBK034026C. Heme oxygenase-1 (HMOX-1) is a marker of oxidative stress upregulated in response to agents that induce oxidative injury [36], and the cytotoxic effects of oxidative stress were exacerbated in cells lacking HMOX-1 [37]. Indeed, when we treated cells with CBK034026C, upregulation of HMOX-1 was observed but the elevation was much weaker in $NAT2^{rapid}$ compared to $NAT2^{slow}$ cells in both RKO and DLD-1 genetic backgrounds (Fig. 4E), supporting that CBK034026C induces oxidative stress which is less efficiently handled in $NAT2^{rapid}$ cells. Since the mitochondrion is the main site for ATP synthesis and inhibition of the Na^+/K^+-ATPase by ouabain was observed to decrease intracellular level of ATP [38], we measured the intracellular ATP level in cells treated with ascending concentrations of CBK034026C or its analogue CBK034296T. Interestingly, at 5 μM, impaired energy production was only noticed in $NAT2^{rapid}$ but not $NAT2^{slow}$ cells (Fig. 4F), indicating that reprogramming of mitochondrial metabolism by differential NAT2 activity could also affect cellular ATP levels.

2.5. Compound CBK034026C and its analog affect the activity of the Nf-kB signaling pathway

It is known that ATPase inhibitors such as ouabain activate the Nf-kB pathway [39,59]. We observed near 4-fold increase of p-Nf-kB after ouabain treatment (Fig. 5A). Moreover, activation of the Nf-kB pathway regulates genes promoting cellular survival. For example, Nf-kB activity can regulate reactive oxygen species (ROS) levels by increasing expression of antioxidant proteins, such as HMOX-1 to protect cells from oxidative stress induced cell death [40,41]. Since we observed an upregulation of HMOX-1 in cells treated with CBK034026C which shows a similar mechanism of action to ATPase inhibitors, we speculated that CBK034026C might as well be able to upregulate Nf-kB pathway. To test this hypothesis, we treated $NAT2^{rapid}$ and $NAT2^{slow}$ cells with increasing concentrations of CBK034026C for 24 h, and observed a significant increase of p-Nf-kB in both RKO and DLD-1 cells (Fig. 5B). Interestingly, compared to RKO cells, DLD-1 cells show a greater induction in both $NAT2^{rapid}$ and $NAT2^{slow}$ cells (in RKO cells, the fold change of p-Nf-kB / t-Nf-kB is ~1.2 whereas in DLD-1 cells the fold change of p-Nf-kB / t-Nf-kB is ~3–4. This may as well explain why DLD-1 cells are less sensitive than RKO cells to CBK034026C and its analogues.

3. Discussion

Novel targeted therapies for treating CRC have been limited by drug resistance, thereby reducing their clinical utility. Loss of heterozygosity (LOH) was originally observed using polymorphic markers which were heterozygous in germline DNA but homozygous in the tumor, and is common during the evolution of cancers [42]. When a bystander gene encoding an essential protein undergoes LOH, further inhibition or loss of the retained allele is lethal to tumor cells whereas normal cells survive relying solely on the remaining allele [43]. Such vulnerabilities created by LOH can provide collateral lethality targets for cancer therapy. Among non-essential genes frequently subject to LOH in cancer, we have previously demonstrated that loss of arylamine *N*-acetyltransferase 2 (NAT2) activity following LOH at 8p22 can be targeted using the cytotoxic kinase inhibitor APA. Here, we performed *de novo* a 33,000-compound screen to find additional potential drug candidates with better safety profile. Unexpectedly, no compounds superior to APA were discovered, but rather a family of compounds selectively killing cells with high NAT2 activity. Hit compounds CBK034026C and its analogue CBK034296T were not direct NAT2 substrates, although we have not excluded the possibility that they are NAT2 substrates after metabolism by phase I enzymes.

Interestingly, our further analyses showed that the transcriptional signature characterizing the response to CBK034026C and its analogue CBK034296T bore the highest similarity to that of Na^+/K^+-ATPase inhibitors, which was further supported by their inhibition of ATPase activity. The most eminent pharmacological function of Na^+/K^+-ATPase inhibitors is improved myocardial contractility in pathologic conditions such as congestive heart failure. In recent years, inhibitors of Na^+/K^+-ATPase have also been reported to exhibit anti-cancer potential *in vitro* and *in vivo*, but the underlying mechanism is not known [44,45]. Here, the novel Na^+/K^+-ATPase inhibitors showed NAT2 activity dependent toxicity and induced greater short-term activation of Nf-kB pathway in cells with rapid NAT2, providing a novel perspective to understand the mechanism underlying the anticancer activity of Na^+/K^+-ATPase inhibitors.

Furthermore, a metabolomic analysis revealed that pathways involved in antioxidant defense (glutathione metabolism) were significantly upregulated in cells harboring slow NAT2 activity. Since glutathione *S*-transferases (GSTs) and *N*-acetyltransferases are multifunctional enzymes that play important roles in phase II cellular

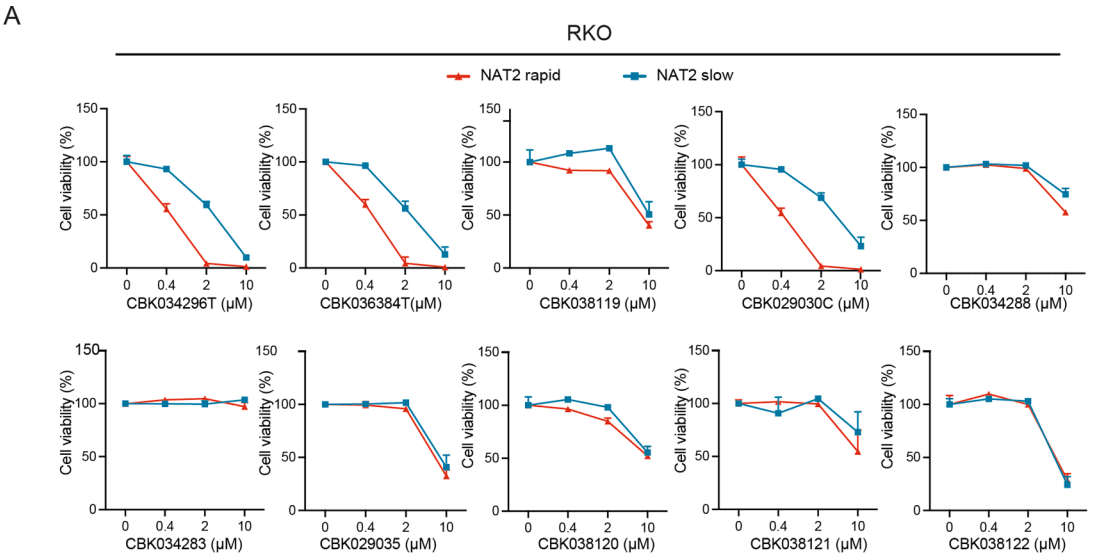

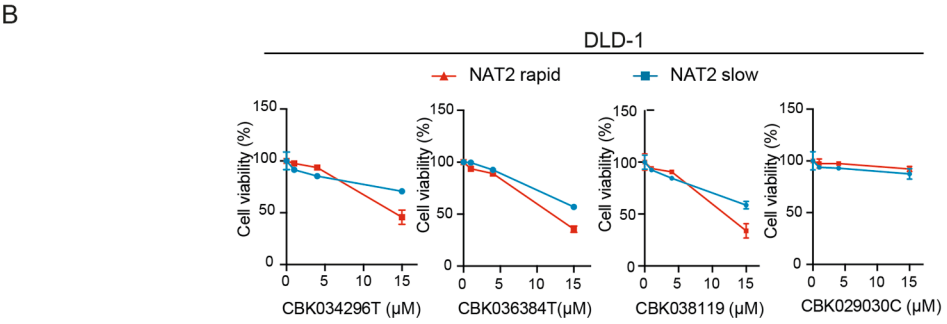

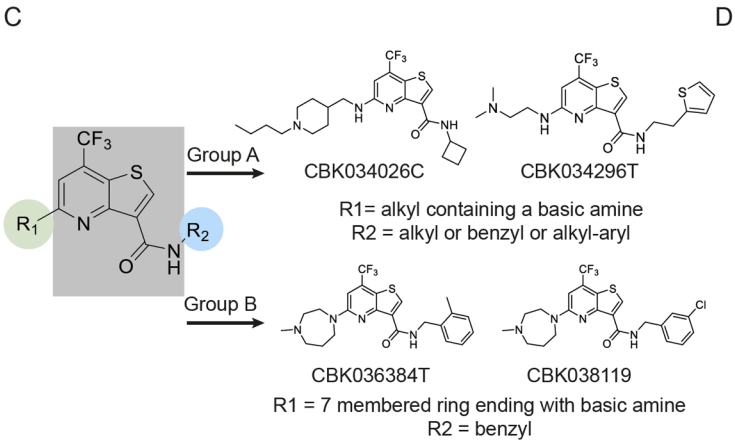

D

R1 and R2 structure of CBK034026C and its analogues

Compound	R1	R2
CBK034026C		
CBK034296T		
CBK036384T		
CBK038119		

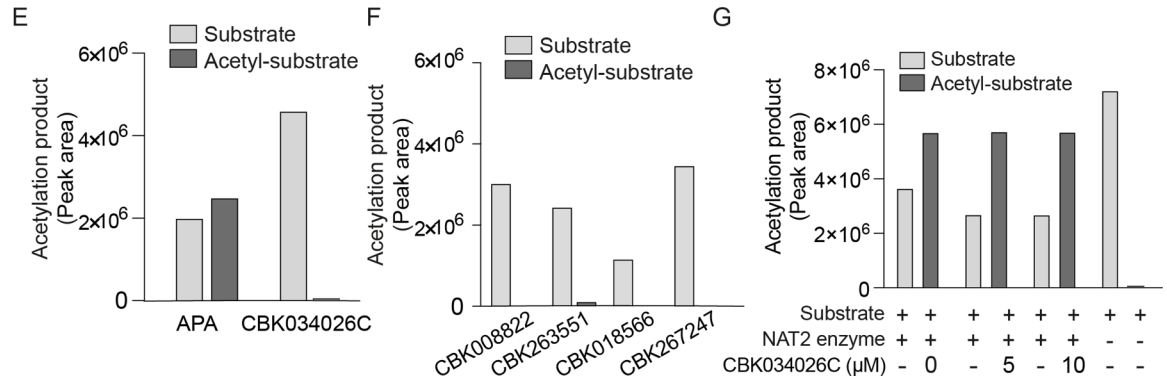

(caption on next page)

Fig. 2. CBK034026C and analogues display NAT2 activity dependent cytotoxicity. A and B. 10 analogues of CBK034026C were found through a structure-based search and tested in RKO NAT2^{rapid} and NAT2^{slow} cells. CBK034296T, CBK036384T and CBK038119 compounds displayed a consistent response pattern with enhanced toxicity to NAT2^{rapid} cells in both RKO and DLD-1 *in vitro* models. The data are expressed as the mean ± SD of three independent experiments. C. The core structures of CBK034026C and its analogs. CBK034026C, CBK034296T, CBK036384T and CBK038119 share the same backbone (gray), R1 (light green) and R2 (light blue) indicating substructures that contribute to cytotoxic effect. Based on the different compositions of R1 and R2, CBK034026C, CBK034296T, CBK036384T and CBK038119 can be further divided into two groups. Group A contains CBK034026C and CBK034296T characterized by R1 = alkyl containing a basic amine and R2 = alkyl or benzyl or alkyl-aryl; Group B contains CBK036384T and CBK038119 characterized by R1 = 7 membered ring ending with basic amine and R2 = benzyl. D. Detailed explanation of the structure of R1 and R2 for CBK034026C and its analogues. E. Quantification of acetylated product from CBK034026C catalyzed by NAT2 enzyme. After 18 h incubation with recombinant NAT2 protein, the corresponding acetylated product for the positive control APA but not CBK034026C was observed. F. Quantification of acetylated product from CBK008822, CBK263551, CBK018566 and CBK267247 catalyzed by NAT2. No acetylated product was detected after 18 h incubation with recombinant NAT2 protein. G. Detection of acetylated product from a known NAT2 substrate (APA) in the absence or presence of CBK034026C. After 18 h incubation of APA with CBK034026C, acetylated product from APA was still present.

detoxification and bioactivation reactions, they are generally considered to be antioxidant enzymes [46]. Hypothetically, cancer cells only retaining slow NAT2 activity may upregulate GST activity to maintain detoxification and bioactivation functions. This could explain why CBK034026C induced oxidative stress and cells lacking NAT2 activity exhibited a stronger protective response measured as the expression level of HMOX-1 and a higher survivability. The increased expression of antioxidant protein HMOX-1 further supports our observation on Nf-kB induction, which is one of the upstream regulators of antioxidant proteins to further protect cells from oxidative stress induced cell death [40,47]. This may also shed a light on understanding the cytotoxic effect of Na^+/K^+-ATPase inhibitors observed in cancer cells, which exhibit aberrant redox homeostasis [48].

Na^+/K^+-ATPase inhibitor digoxin is one of the oldest cardiovascular medications used today. It is classified as a cardiac glycoside and was initially approved by the FDA in 1954 [49]. In 2019, there are more than 2 million prescriptions in the USA (clincalc.com). Currently, there are 29 clinical trials of digoxin in the treatment of cancer (clinicaltrials.gov), For example, in clinical trial NCT01763931 with a purpose to study effects of digoxin on breast cancer, no serious adverse effects were observed, but other adverse effects were recorded, such as ear pain, dry mouth, cellulitis (https://clinicaltrials.gov/ct2/show/NCT01763931 and http://www.cdek.liu.edu/trial/NCT01763931/0. In clinical trial NCT01162135 with a purpose to study effects of digoxin on recurrent prostate cancer, digoxin was well tolerated with possible relation of one grade 3 back pain. No patients had evidence of digoxin toxicity (https://clinicaltrials.gov/ct2/show/study/NCT01162135) [50]. Adverse effects might as well happen to our identified new Na^+/K^+-ATPase inhibitors, however, since CBK034026C and its analogues CBK034296T, CBK036384T and CBK038119 displayed a consistent response pattern with enhanced toxicity to NAT2^{rapid} cells in both RKO and DLD-1 *in vitro* models. We hope that at least one of them may have efficient therapeutic effect as well as a safe profile in preclinical models.

In this study, we also noticed that, compared to DLD-1 cells, RKO cells exhibit greater selection capacity in the 33,000-compound screen. For example, CBK263551 and CBK267247 were confirmed as hit compounds in RKO cell model but not in DLD-1 cell model. In our previous study, NAT2 activity was measured in both DLD-1 and RKO cell models. We noticed that compared to DLD-1, RKO cells displayed higher basal NAT2 catalytic activity, even as the acetylation activities were ≥8-fold higher in rapid NAT2 clones when compared to slow NAT2 in both RKO and DLD-1 cells [17]. Since CBK263551 and CBK267247 are not direct substrates of NAT2, RKO cells may have a greater selectivity in the drug screen performed here. At the same time, studies have observed altered expressions of Na^+/K^+-ATPase subunits in CRC [51,52] and distinct affinities for ouabain in heterologous Na^+/K^+-ATPase systems [53]. This may partially explain why Na^+/K^+-ATPase inhibitor CBK034026C and its analogues could be selected from both DLD-1 and RKO cell models. However, the underlying mechanism is still unclear and warrants further investigation. Further, CBK034026C displayed stronger inhibition of Na^+/K^+-ATPase in DLD-1 cells but a greater cytotoxic effect in RKO cells suggesting that CBK034026C toxicity is not solely stemming from the inhibition of ATPase activity. The degree of oxidative stress, changes in intracellular ATP levels, and extent of Nf-kB pathway induction may as well affect CBK034026C induced cell death. Together with the mechanism of action data obtained from C-MAP analysis, CBK034026C may have multiple targets, a common observation in drug discovery [54]. Therefore, further optimization of the structure of CBK034026C may be required.

The rapid acetylator phenotype has been linked to an increased risk of colorectal cancer through producing ROS, which can form irreversible DNA adducts [55] and trigger oxidative stress [56]. Recently, we discovered that also endogenous aliphatic amines could be acetylated by NAT2 [26], supporting a role in cellular metabolism beyond xenobiotic metabolism. The findings here provide novel tools to dissect and understand the effect of NAT2 on intracellular metabolism. Further, they provide insights for development of novel anticancer agents for CRC patients whose tumors have high NAT2 activity. Combined with APA or other agents that exhibit preferential toxicity to NAT2^{slow} cells, CRC patients whose tumors retain solely rapid (16%) or slow NAT2 allele (61%) after 8p22 LOH [25] could benefit from NAT2 activity-targeted treatment, which warrants further investigation.

4. Materials and methods

4.1. Cell culture

Parental RKO (#CRL-2577) and DLD-1 (#CCL-221) cells were obtained from ATCC (Manassas, VA, USA). RKO and DLD-1 NAT2^{rapid} and NAT2^{slow} cells were established in our group and characterised, information in detail can be found in [17]. All cells were maintained in McCoy's 5A medium (#16600082, Thermo Scientific, Waltham, MA, USA) with the addition of 10% Fetal Bovine Serum (Thermo Scientific, Waltham, MA, USA) and 1% Penicillin-Streptomycin (Thermo Scientific, Waltham, MA, USA) at 37 °C in 5% CO_2. All cell lines were authenticated by STR profiling (ATCC cell authentication service) and regularly checked for mycoplasma infection with MycoAlert mycoplasma detection kit (Lonza, Basel, Switzerland).

4.2. Drug screening

4.2.1. Screening library, plate layout and procedure

The screen was performed in 384w format using ~33 k CBCS primary screening set at 10 μM (Library description: https://compoundcenter.scilifelab.se/file/library_description, Library download: https://figshare.com/s/17d8acfc882994e44468). The compounds were donated by various biotech companies and originates from both in-house and commercial sources. Compounds included in the primary screening set were selected to represent a diverse selection of a larger set of >350,000 compounds, while keeping a certain depth to allow crude structure–activity relationship studies.

Compounds (10 mM in DMSO) were spotted in assay ready plates (NUNC TC black optical bottom 384w plates) with the echo dispenser at CBCS to a final volume of 60 nl per well, and 60 nl of DMSO was spotted in control wells. RKO NAT2^{slow} cells were seeded in 60 μl McCoy's 5A medium supplemented with 10% FBS and 1% Pen-Strep, at a density of

A

Mechanism of Action Rank List

Rank	CBK034026C	fdr_q_nlog10
1	**ATPase inhibitor**	1.68
2	Tubulin inhibitor	1.43
3	NFkb pathway inhibitor	0.91
4	Microtubule inhibitor	0.86
5	Proteasome inhibitor	0.86
6	HDAC inhibitor	0.84
7	Tyrosine kinase inhibitor	0.84
8	Histamine receptor agonist	0.83
9	Protein synthesis inhibitor	0.83
10	VitaminD receptor agonist	0.80

B

Mechanism of Action Rank List

Rank	CBK034296T	fdr_q_nlog10
1	**ATPase inhibitor**	3.29
2	Protein synthesis inhibitor	3.14
3	HDAC inhibitor	3.11
4	Adenylyl cyclase activator	1.93
5	mTOR inhibitor	1.92
6	Androgen receptor antagonist	1.90
7	AKT inhibitor	1.80
8	NFkB pathway inhibitor	1.76
9	Na/Ca exchange inhibitor	1.71
10	Sterol demethylase inhibitor	1.67

C

Top 10 referenced compounds (set of ATPase inhibitor)

Rank	Score	Name	Description
1	96.3	digitoxin	ATPase inhibitor
2	94.86	digoxin	ATPase inhibitor
3	94.29	proscillaridin	ATPase inhibitor
4	93.97	digitoxigenin	ATPase inhibitor
5	93.66	strophanthidin	ATPase inhibitor
6	93.21	helveticoside	ATPase inhibitor
7	92.32	ouabain	ATPase inhibitor
8	92.07	bufalin	ATPase inhibitor
9	90.98	cinobufagin	ATPase inhibitor
10	67.45	oligomycin-a	ATP synthase inhibitor

D

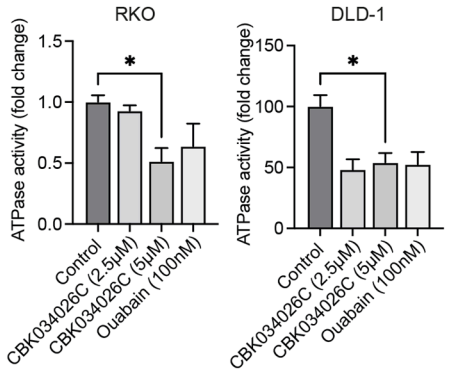

E

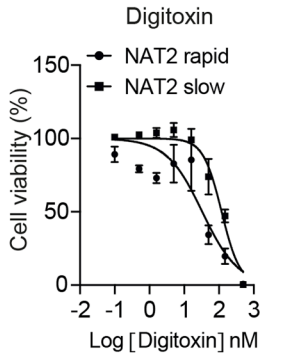

	Rapid	Slow
IC50	33.05	119.2

F

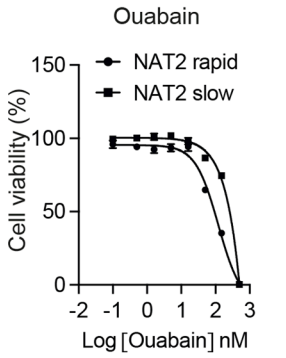

	Rapid	Slow
IC50	84.30	196.4

Fig. 3. Compound CBK034026C and its analogue CBK034296T elicit similar cellular effects as the Na^+/K^+-ATPase inhibitors. For Connectivity Map (CMap) analysis, MCF7 cells were incubated with CBK034026C or its analogue CBK034296T for 6 h, RNA extracted and subject to gene expression analysis. A and B. Ranked mechanism of action list for CBK034026C and CBK034296T from CMap analysis. C. Top 10 ranked compounds belonging to the perturbagens of ATPase inhibitors provided by the CMap LINCS resource (https://clue.io). D. ATPase enzyme activity was measured in RKO and DLD-1 parental cells treated with CBK034026C (2.5 μM and 5.0 μM) or ouabain (100 nM). ATPase enzyme activity was shown as fold change treated versus DMSO control. The data are expressed as the mean ± SD of three independent experiments (n = 3, * $P < 0.05$ by two-tailed *t*-test). E. Cell viability was measured in $NAT2^{rapid}$ and $NAT2^{slow}$ cells after 72 h incubation with known ATPase inhibitors digitoxin and ouabain. The data are expressed as the mean ± SD of three independent experiments (n = 5).

2400 cells per well in assay ready plates and incubated at 37 °C, 5% CO_2. After 72 h, 6 μl of resazurin per well was added using the BioMek Nx robot. Cells were incubated with resazurin for 2 h at 37 °C, 5% CO_2 after which fluorescence (535x/590 m) was measured. The assay was rather stable with Z'-values between 0.76 and 0.84. To normalize data, % viability was calculated for each datapoint as fluorescence units (FU) at 590 nm for compound/FU DMSO control in respective plate. Compounds with >20% decreased viability over DMSO control were selected for counter screen on RKO cells with rapid NAT2 activity.

4.2.2. Hit selection

A set of 704 compounds with >20% cytotoxicity towards cells with slow NAT2 activity were progressed to hit selection. To verify expected NAT2 expression differences, APA-cytotoxicity were determined prior to the experiment. Compounds were tested at 3 concentrations (10, 5 and 1.25 μM) spotted in columns starting with 10 μM. This layout made up 6

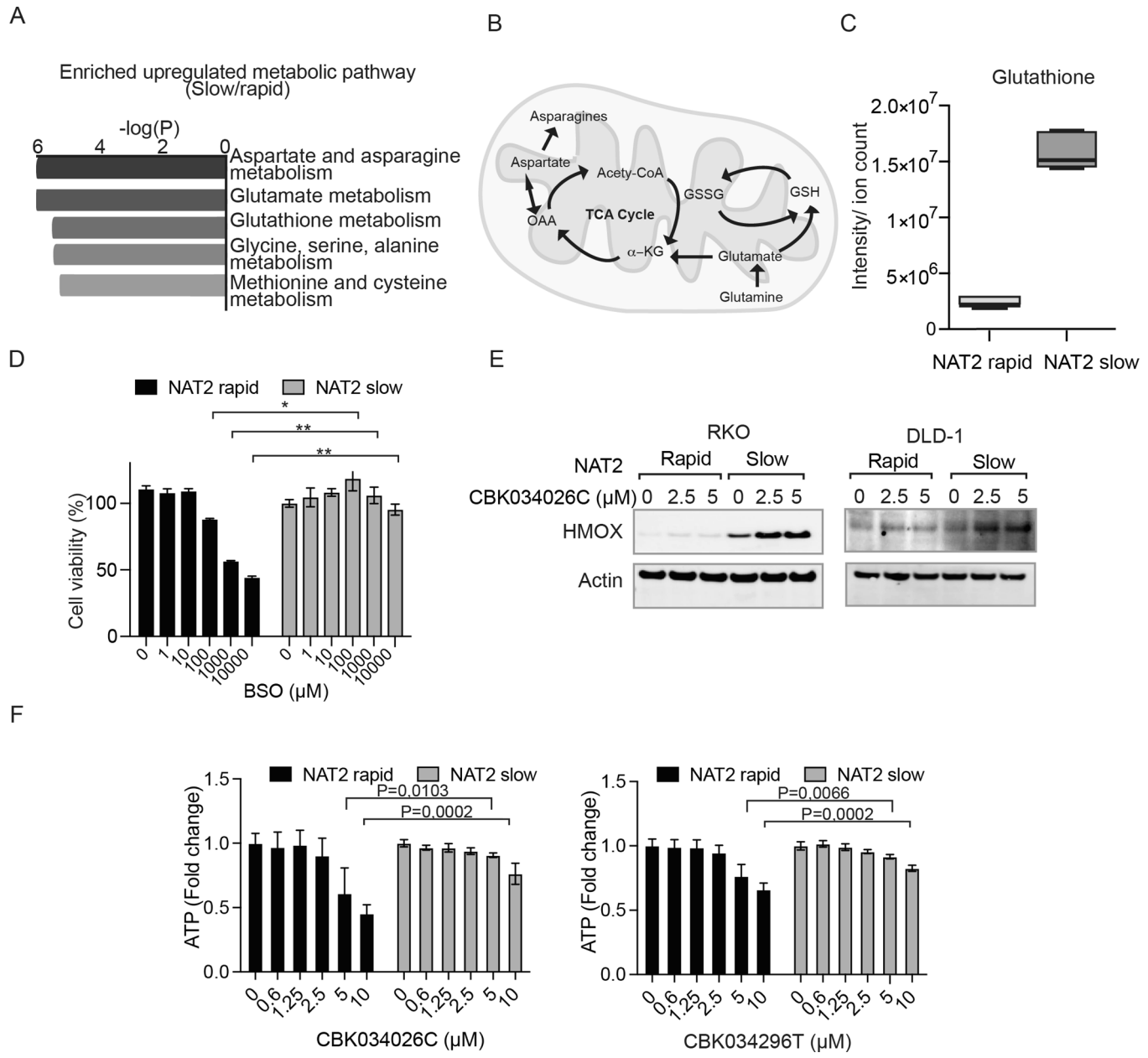

Fig. 4. Reprograming of mitochondrial metabolism by NAT2. A. Enrichment analysis of altered metabolic pathway in NAT2^{slow} compared to NAT2^{rapid} RKO cells. B. Schematic illustrating how these three pathways are involved in mitochondrial activity. Asparagine and aspartate metabolism is a critical source of energy, building blocks of protein synthesis and signaling molecules. Glutamine is the major source of cellular nitrogen for *de novo* biosynthesis of nucleotides and other nonessential amino acids. Glutamate is also utilized to synthesize the antioxidant glutathione and is an important energy source via mitochondrial glutaminolysis. OAA: oxaloacetic Acid, α-KG: alpha-Ketoglutarate, GSSG: glutathione disulfide, GSH: glutathione, TCA cycle: tricarboxylic acid cycle. C. Glutathione amount was measured by intensity/ion count through tandem mass spectrometry (MS/MS). D. Cell viability of RKO NAT2^{rapid} and NAT2^{slow} cells after 72 h treatment with indicated concentrations of BSO. The data are expressed as the mean ± SD of three independent experiments (n = 3, *P < 0.05, ** P < 0.01 and *** P < 0.001 by Student's unpaired Two-stage step-up *t* test). E. Expression levels of HMOX in RKO NAT2^{rapid} and NAT2^{slow} cells exposed to the indicated concentrations of CBK034026C for 24 h. F. Intracellular ATP levels were measured in RKO NAT2^{rapid} and NAT2^{slow} cells exposed to the indicated concentrations of CBK034026C and CBK034296T for 6 h. Thereafter, fold change (treated/DMSO) under each condition was calculated. The data are expressed as the mean ± SD of three independent experiments (n = 3), *P < 0.05, ** P < 0.01 and *** P < 0.001 by Student's unpaired Two-stage step-up *t* test.

full individual plates with 704 compounds of which one copy per cell line were tested in parallel on RKO NAT2^{slow} or NAT2^{rapid} cells respectively. The stability was similar to those obtained in the screen with plate Z'-values ranging from 0.77 to 0.88. For selection of hits, the ratio in viability between two cell types was calculated as % viability of RKO NAT2^{rapid} cells divided by % viability of RKO NAT2^{slow} cells (H/e). Compounds with selective toxicity towards either cell-line, based on ratio in % viability, were selected for further verification studies. After this step, 332 compounds out of 704 were selected for hit confirmation.

4.2.3. Hit confirmation

The 332 hits were grouped according to level of toxicity detected during hit selection, and the concentration interval was optimized for each group as follows. a). Highly toxic compounds were titrated 11 steps (5 μM – 1 nM or 2.5 μM – 0.5 nM). b). Compounds with toxicity interval in range with hit selection concentration were titrated in 3 steps from 10 μM – 2.5 μM or in 4 steps from 10 μM – 1.25 μM depending on the results from hit selection. c). Compounds with low toxicity were titrated in 3 steps from 20 μM – 5 μM or in 4 steps from 20 μM – 2.5 μM. Culture

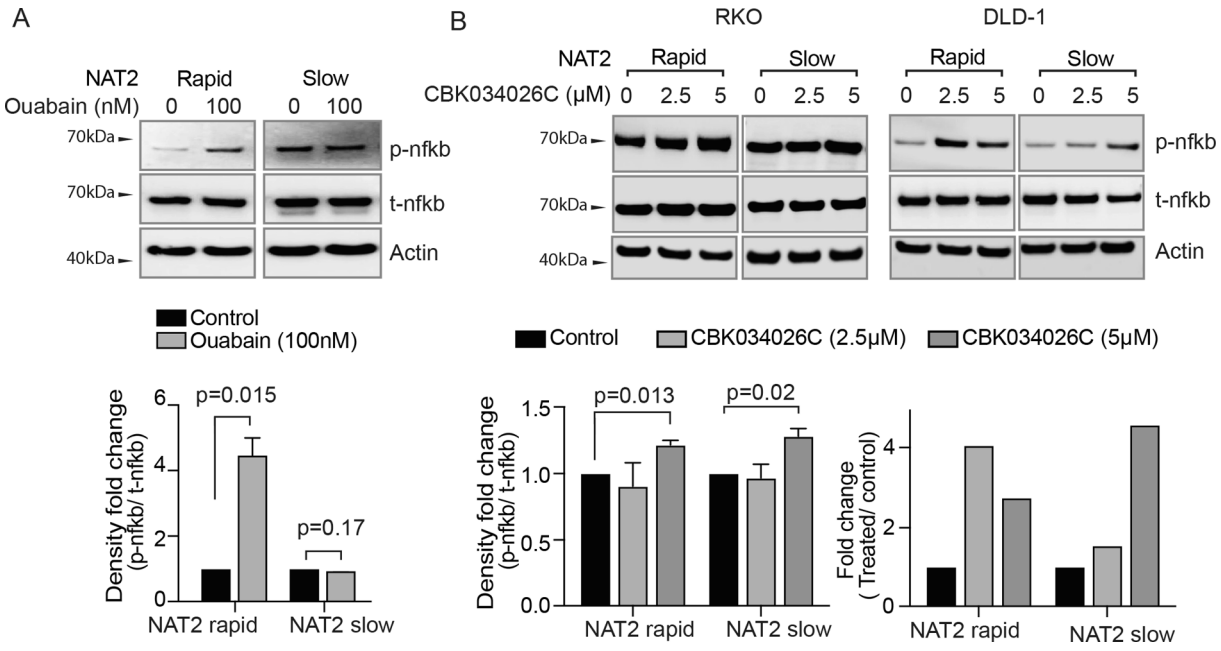

Fig. 5. Compound CBK034026C and its analog affect the activity of the Nf-kB signaling pathway. A. Protein expression of phospho-Nf-kB and total-Nf-kB in NAT2^{rapid} and NAT2^{slow} RKO cells exposed to 100 nM ouabain for 24 h. The density fold change is shown as the mean ± SD of three independent experiments, P value was indicated in the figure. B. Expression of phospho-Nf-kB and total-Nf-kB in NAT2^{rapid} and NAT2^{slow} cells exposed to CBK034026C for 24 h.

conditions and calculation were the same as optimized for the screen with plate Z'-values ranging from 0.67 to 0.83. After this step, 36 compounds out of 332 were selected for the next full-dose response test. Full-dose response (DR) test was performed at 11 concentrations ranging from 48 μM-5 nM (n = 3) for selected hits and their analogues, and from 5 μM-0.5 nM (n = 3) for compounds with high toxicity. The DR experiment was performed as described for the screen. After this step, 9 compounds out of 36 were confirmed as hits (APA was reidentified from this screen).

4.3. Connectivity map analysis

MCF-7 cells were used since it is the most frequently used cell model in the Connectivity Map database. Here, MCF-7 cells were seeded into 6-well plates at a density of 300,000 cells per well. Next day, cells were treated with CBK034026C and its analogue CBK034296T for 6 h. After the treatment, cells were washed once with PBS. Afterwards, PBS was removed and cell pellets were collected for RNA extraction which was performed using RNeasy Mini Kit (Qiagen) followed by the L1000, a relatively inexpensive and rapid high-throughput gene expression profiling technology. Briefly, expression data in response to CBK034026C and its analogue CBK034296T were processed through a computational pipeline that converts raw fluorescence intensity into signatures, which can be used to query the Connectivity Map database for perturbations that give a related gene expression response.

4.4. UPLC-MS analysis

Ultra-high-performance liquid chromatography coupled to mass spectrometry (UPLC-MS) was used for metabolomics analysis. Mass spectrometric analysis was performed on an Acquity UPLC system connected to a Synapt G2 Q-TOF mass spectrometer, both from Waters Corporation (Milford, MA, USA). The system was controlled using the MassLynx software package v 4.1, also from Waters. The separation was performed on an Acquity UPLC® BEH C18 column (1.7 μm, 100 × 2.1 mm) or an Acquity UPLC® HSS T3 column (1.8 μm, 100 × 2.1 mm) from Waters Corporation. The mobile phase consisted of a combination of 0.1% formic acid in MilliQ water (A) and 0.1% formic acid in LC-MS grade methanol (B). The column temperature was 40 °C and the mobile phase gradient applied was as follows: 0–8.5 min, 0–100 % B; 8.5–10 min, 100 % B; 10–12 min, 100–0 % B; 12–17 min, 0 % B, with a flow rate of 0.3 ml/min. The samples were introduced into the q-TOF using positive electrospray ionization. The capillary voltage was set to 2.50 kV and the cone voltage was 40 V. The source temperature was 100 °C, the cone gas flow 50 l/min and the desolvation gas flow 600 l/h. The instrument was operated in MSE mode, the scan range was m/z = 50–1200, and the scan time was 0.3 s. A solution of sodium formate (0.5 mM in 2-propanol: water, 90:10, v/v) was used to calibrate the instrument and a solution of leucine-encephalin (2 ng/μl in acetonitrile: 0.1% formic acid in water, 50:50, v/v) was used for the lock mass correction at an injection rate of 30 s.

4.5. Metabolite identification

The XCMS software package [57] was used to perform peak identification, retention time correction, and peak integration yielding a list of identified peaks by increasing p-value, which were then corrected for multiple comparisons (FDR). Identification of the features was performed by comparing their m/z ratios to a list of exact masses for known human endogenous metabolites from the human metabolome database (HMDB) with a mass spectrometric accuracy < 10 ppm.

4.6. Metabolic pathway analysis

The Mummichog2 software package [58] was used for the identification of altered metabolic pathways between mutants and their corresponding control cell lines. The pathway analysis was performed through integration of both negative and positive mode mass spectrometric analysis to ensure high metabolite pathway coverage. The results from both analytical models were combined using Fisher's method to find the X^2 value for each pathway, which was then converted into the z-value.

$$X_4^2 \sim -2ln(p_+) - 2ln(p_-)$$

4.7. ATPase activity assay

ATPase Assay Kit (#ab234055) was used as recommended by the manufacturer (Abcam, Cambridge, UK). Briefly, RKO and DLD-1 cells were plated in 60 mm cell culture dishes (VWR) at a density of 2×10^6 cells per dish and incubated at 37 °C overnight. Next day, cells were treated with 2.5 μM and 5 μM of CBK034026C or 100 nM of Ouabain Octahydrate (#HY-B0542, MedChemExpress, Monmouth Junction, USA) and incubated at 37 °C for 6 h. Samples were then washed once with 1x HBSS (Thermo Scientific, Waltham, MA, USA), lysed with ice cold ATPase assay buffer and placed on ice for 10 min, before centrifugation at 10.000 g at 4 °C for 10 min. Supernatants, phosphate standards, reagent control and ATPase positive controls were added to the 96-well plate as duplicates. The reaction mix was added to the wells that contain positive control, reagent control and test samples; while background control mix was added to sample background controls. The plate was incubated at 25 °C for 30 min. ATPase assay developer was added to standard, control and sample wells. The plate was incubated at 25 °C for 30 min, before OD measurement at 650 nm in endpoint mode at Synergy HTX reader.

4.8. CellTiter-Glo® Luminescent ATP measurement

The CellTiter-Glo® Luminescent Cell Viability Assay (#G9681, Promega, Madison, USA) was used. Briefly, RKO NAT2^{rapid} and NAT2-^{slow} cells were plated in opaque-walled 96-well plates at a density of 15,000 cells per well and incubated at 37° C overnight. Control wells were prepared only with McCoy's 5A complete medium (Thermo Scientific, Waltham, MA, USA). Next day, cells were treated with 0.6 μM, 1.25 μM, 2.5 μM, 5 μM and 10 μM of CBK034026C and CBK034296T. The plates were incubated for 1 h or 6 h at 37 °C and placed at room temperature for 30 min. CellTiter-Glo® Reagent was added to each well. The plates were placed on an orbital shaker for 2 min and incubated at room temperature for 10 min. Luminescence was recorded using CLARIOstar Plus.

4.9. Glutathione depletion treatment

RKO NAT2^{rapid} and NAT2^{slow} cells were plated in a 96-well plate at a density of 8,000 cells per well and incubated at 37 °C overnight. Next day, cells were treated with different concentrations (10 μM, 50 μM, 100 μM, 250 μM, 500 μM, 1 mM) of BSO (L-Buthionine sulphoximine). After 72 h, cell medium was replaced with 1x resazurin (#R7017, Sigma-Aldrich, St. Louis, MO, USA) and the plate was incubated at 37 °C for 2 h. Fluorescence intensity was read at Synergy HTX with 530/25 nm excitation and 590/35 nm emission.

4.10. Western blot

Cells were collected and lysed in ice-cold lysis buffer and run on 4–12% SDS-PAGE gels (#NP0336BOX, Thermo Scientific, Waltham, MA, USA). Proteins were transferred to nitrocellulose membranes and incubated at room temperature in 5% non-fat dry milk in 1x PBST for 1 h. Membranes were then incubated overnight at 4 °C with primary antibodies HMOX1 (#MA1-112, Mouse, Thermo Scientific, Waltham, MA, USA), β-Actin (#sc-47778, Mouse, Santa Cruz Biotechnology, TX, USA), p-NF-κB (#3033, Rabbit, Cell Signaling, Denvers, MA, USA), NF-κB (#3034, Rabbit, Cell Signaling, Denvers, MA, USA) and Cleaved Caspase-3 (#9664, Rabbit, Cell Signaling, Denvers, MA, USA) at a dilution of 1:1000 in 1x PBST. Next day, membranes were washed with 1x PBST and incubated with anti-Rabbit (#31430, Thermo Scientific, Waltham, MA, USA) or anti-Mouse secondary antibodies (#31460, Thermo Scientific, Waltham, MA, USA) at a dilution of 1:5000 for 1 h. Immunoreactive bands were detected by FluorChem Fluorescent Western Imaging System from ProteinSimple.

CRediT authorship contribution statement

Xiaonan Zhang: Formal analysis, Data curation, Writing - original draft, Writing - review & editing. **Ece Akcan:** Formal analysis, Data curation, Writing - original draft, Writing - review & editing. **Mario Correia:** Formal analysis, Data curation, Writing - review & editing. **Natallia Rameika:** Methodology, Writing - review & editing. **Snehangshu Kundu:** Formal analysis, Methodology, Writing - review & editing. **Ivaylo Stoimenov:** Methodology, Writing - review & editing. **Veronica Rendo:** Methodology, Writing - review & editing. **Anna U. Eriksson:** Formal analysis, Data curation, Writing - review & editing. **Martin Haraldsson:** Resources, Writing - original draft, Writing - review & editing. **Daniel Globisch:** Funding acquisition, Methodology, Resources, Writing - review & editing. **Tobias Sjöblom:** Conceptualization, Funding acquisition, Funding acquisition, Methodology, Resources, Supervision, Writing - original draft, Writing - review & editing.

Declaration of Competing Interest

The authors declare that they have no known competing financial interests or personal relationships that could have appeared to influence the work reported in this paper.

Acknowledgements

This study was supported by grants from Cancerfonden (T.S., grant reference CAN 2018/772 and 211719 Pj 01H), Vetenskapsrådet (T.S., grant reference 2020-02371 and D.G., grant reference 2020-04707), Erling-Perssons stiftelse (T.S.).

References

[1] H. Sung, J. Ferlay, R.L. Siegel, M. Laversanne, I. Soerjomataram, A. Jemal, F. Bray, Global cancer statistics 2020: GLOBOCAN estimates of incidence and mortality worldwide for 36 cancers in 185 countries, CA Cancer. J. Clin (2021).
[2] D.P. Modest, S. Pant, A. Sartore-Bianchi, Treatment sequencing in metastatic colorectal cancer, Eur. J. Cancer 109 (2019) 70–83.
[3] K. Van der Jeught, H.C. Xu, Y.J. Li, X.B. Lu, G. Ji, Drug resistance and new therapies in colorectal cancer, World. J. Gastroenterol. 24 (34) (2018) 3834–3848.
[4] R. Capdeville, E. Buchdunger, J. Zimmermann, A. Matter, Glivec (STI571, imatinib), a rationally developed, targeted anticancer drug, Nat. Rev. Drug. Discov. 1 (7) (2002) 493–502.
[5] D.R. Camidge, W. Pao, L.V. Sequist, Acquired resistance to TKIs in solid tumours: learning from lung cancer, Nat. Rev. Clin. Oncol. 11 (8) (2014) 473–481.
[6] D.Y. Oh, Y.J. Bang, HER2-targeted therapies - a role beyond breast cancer, Nat. Rev. Clin. Oncol. 17 (1) (2020) 33–48.
[7] B. Vogelstein, N. Papadopoulos, V.E. Velculescu, S. Zhou, L.A. Diaz Jr., K. W. Kinzler, Cancer genome landscapes, Science 339 (6127) (2013) 1546–1558.
[8] M.T. Villanueva, Long path to MYC inhibition approaches clinical trials, Nat. Rev. Drug. Discov. (2019).
[9] G. Zinzalla, Targeting MYC: is it getting any easier? Future. Med. Chem. 8 (16) (2016) 1899–1902.
[10] A.R. Moore, S.C. Rosenberg, F. McCormick, S. Malek, RAS-targeted therapies: is the undruggable drugged? Nat. Rev. Drug. Discov. 19 (8) (2020) 533–552.
[11] G.V. Kryukov, F.H. Wilson, J.R. Ruth, J. Paulk, A. Tsherniak, S.E. Marlow, F. Vazquez, B.A. Weir, M.E. Fitzgerald, M. Tanaka, C.M. Bielski, J.M. Scott, C. Dennis, G.S. Cowley, J.S. Boehm, D.E. Root, T.R. Golub, C.B. Clish, J.E. Bradner, W.C. Hahn, L.A. Garraway, MTAP deletion confers enhanced dependency on the PRMT5 arginine methyltransferase in cancer cells, Science 351 (6278) (2016) 1214–1218.
[12] F.L. Muller, S. Colla, E. Aquilanti, V.E. Manzo, G. Genovese, J. Lee, D. Eisenson, R. Narurkar, P. Deng, L. Nezi, M.A. Lee, B. Hu, J. Hu, E. Sahin, D. Ong, E. Fletcher-Sananikone, D. Ho, L. Kwong, C. Brennan, Y.A. Wang, L. Chin, R.A. DePinho, Passenger deletions generate therapeutic vulnerabilities in cancer, Nature 488 (7411) (2012) 337–342.
[13] P. Dey, J. Baddour, F. Muller, C.C. Wu, H. Wang, W.T. Liao, Z. Lan, A. Chen, T. Gutschner, Y. Kang, J. Fleming, N. Satani, D. Zhao, A. Achreja, L. Yang, J. Lee, E. Chang, G. Genovese, A. Viale, H. Ying, G. Draetta, A. Maitra, Y.A. Wang, D. Nagrath, R.A. DePinho, Genomic deletion of malic enzyme 2 confers collateral lethality in pancreatic cancer, Nature 542 (7639) (2017) 119–123.
[14] B.R. Paolella, W.J. Gibson, L.M. Urbanski, J.A. Alberta, T.I. Zack, P. Bandopadhayay, C.A. Nichols, P.K. Agarwalla, M.S. Brown, R. Lamothe, Y. Yu, P. S. Choi, E.A. Obeng, D. Heckl, G. Wei, B. Wang, A. Tsherniak, F. Vazquez, B. A. Weir, D.E. Root, G.S. Cowley, S.J. Buhrlage, C.D. Stiles, B.L. Ebert, W.C. Hahn, R. Reed, R. Beroukhim, Copy-number and gene dependency analysis reveals partial copy loss of wild-type SF3B1 as a novel cancer vulnerability, Elife 6 (2017).

[15] C. Lengauer, K.W. Kinzler, B. Vogelstein, Genetic instabilities in human cancers, Nature 396 (6712) (1998) 643–649.

[16] D.L. Stoler, N. Chen, M. Basik, M.S. Kahlenberg, M.A. Rodriguez-Bigas, N. J. Petrelli, G.R. Anderson, The onset and extent of genomic instability in sporadic colorectal tumor progression, Proc. Natl. Acad. Sci. USA 96 (26) (1999) 15121–15126.

[17] V. Rendo, I. Stoimenov, A. Mateus, E. Sjoberg, R. Svensson, A.L. Gustavsson, L. Johansson, A. Ng, C. O'Brien, M. Giannakis, P. Artursson, P. Nygren, I. Cheong, T. Sjoblom, Exploiting loss of heterozygosity for allele-selective colorectal cancer chemotherapy, Nat. Commun. 11 (1) (2020) 1308.

[18] A. Sabbagh, A. Langaney, P. Darlu, N. Gerard, R. Krishnamoorthy, E.S. Poloni, Worldwide distribution of NAT2 diversity: implications for NAT2 evolutionary history, BMC Genet 9 (2008) 21.

[19] A. Mahasneh, A. Jubaili, A. El Bateiha, M. Al-Ghazo, I. Matalka, M. Malkawi, Polymorphisms of arylamine N-acetyltransferase2 and risk of lung and colorectal cancer, Genet. Mol. Biol. 35 (4) (2012) 725–733.

[20] S.R. Hanson, M.D. Best, C.H. Wong, Sulfatases: structure, mechanism, biological activity, inhibition, and synthetic utility, Angew. Chem. Int. Ed. Engl. 43 (43) (2004) 5736–5763.

[21] B. Lawrence, C. Blenkiron, K. Parker, P. Tsai, S. Fitzgerald, P. Shields, T. Robb, M. L. Yeong, N. Kramer, S. James, M. Black, V. Fan, N. Poonawala, P. Yap, E. Coats, B. Woodhouse, R. Ramsaroop, M. Yozu, B. Robinson, K. Henare, J. Koea, P. Johnston, R. Carroll, S. Connor, H. Morrin, M. Elston, C. Jackson, P. Reid, J. Windsor, A. MacCormick, R. Babor, A. Bartlett, D. Damianovich, N. Knowlton, S. Grimmond, M. Findlay, C. Print, Recurrent loss of heterozygosity correlates with clinical outcome in pancreatic neuroendocrine cancer, NPJ Genom. Med. 3 (2018) 18.

[22] A. Husain, X. Zhang, M.A. Doll, J.C. States, D.F. Barker, D.W. Hein, Identification of N-acetyltransferase 2 (NAT2) transcription start sites and quantitation of NAT2-specific mRNA in human tissues, Drug. Metab. Dispos. 35 (5) (2007) 721–727.

[23] D.W. Hein, M.A. Doll, A.J. Fretland, M.A. Leff, S.J. Webb, G.H. Xiao, U. S. Devanaboyina, N.A. Nangju, Y. Feng, Molecular genetics and epidemiology of the NAT1 and NAT2 acetylation polymorphisms, Cancer Epidemiol. Biomarkers. Prev. 9 (1) (2000) 29–42.

[24] D.M. Grant, N.C. Hughes, S.A. Janezic, G.H. Goodfellow, H.J. Chen, A. Gaedigk, V. L. Yu, R. Grewal, Human acetyltransferase polymorphisms, Mutat. Res. 376 (1–2) (1997) 61–70.

[25] V. Rendo, S. Kundu, N. Rameika, V. Ljungstrom, R. Svensson, K. Palin, L. Aaltonen, I. Stoimenov, T. Sjoblom, Defining eligible patients for allele-selective chemotherapies targeting NAT2 in colorectal cancer, Sci. Rep. 10 (1) (2020) 22436.

[26] L.P. Conway, V. Rendo, M.S.P. Correia, I.A. Bergdahl, T. Sjoblom, D. Globisch, Unexpected Acetylation of Endogenous Aliphatic Amines by Arylamine N-Acetyltransferase NAT2, Angew. Chem. Int. Ed. Engl. 59 (34) (2020) 14342–14346.

[27] A. Subramanian, R. Narayan, S.M. Corsello, D.D. Peck, T.E. Natoli, X. Lu, J. Gould, J.F. Davis, A.A. Tubelli, J.K. Asiedu, D.L. Lahr, J.E. Hirschman, Z. Liu, M. Donahue, B. Julian, M. Khan, D. Wadden, I.C. Smith, D. Lam, A. Liberzon, C. Toder, M. Bagul, M. Orzechowski, O.M. Enache, F. Piccioni, S.A. Johnson, N.J. Lyons, A.H. Berger, A.F. Shamji, A.N. Brooks, A. Vrcic, C. Flynn, J. Rosains, D.Y. Takeda, R. Hu, D. Davison, J. Lamb, K. Ardlie, L. Hogstrom, P. Greenside, N.S. Gray, P.A. Clemons, S. Silver, X. Wu, W.N. Zhao, W. Read-Button, X. Wu, S.J. Haggarty, L.V. Ronco, J.S. Boehm, S.L. Schreiber, J.G. Doench, J.A. Bittker, D.E. Root, B. Wong, T.R. Golub, A Next Generation Connectivity Map: L1000 Platform and the First 1,000,000 Profiles, Cell 171(6) (2017) 1437-1452 e17.

[28] T.V. Seraphim, W.A. Houry, AAA+ proteins, Curr. Biol. 30 (6) (2020) R251–R257.

[29] P.I. Hanson, S.W. Whiteheart, AAA+ proteins: have engine, will work, Nat. Rev. Mol. Cell. Biol. 6 (7) (2005) 519–529.

[30] P.L. Pedersen, Transport ATPases: structure, motors, mechanism and medicine: a brief overview, J. Bioenerg. Biomembr. 37 (6) (2005) 349–357.

[31] L.A. Shchepina, O.Y. Pletjushkina, A.V. Avetisyan, L.E. Bakeeva, E.K. Fetisova, D. S. Izyumov, V.B. Saprunova, M.Y. Vyssokikh, B.V. Chernyak, V.P. Skulachev, Oligomycin, inhibitor of the F0 part of H+-ATP-synthase, suppresses the TNF-induced apoptosis, Oncogene 21 (53) (2002) 8149–8157.

[32] F.I. Marcus, J.N. Ryan, M.G. Stafford, The reactivity of derivatives of digoxin and digitoxin as measured by the Na-K-atpase displacement assay and by radioimmunoassay, J. Lab. Clin. Med. 85 (4) (1975) 610–620.

[33] G.J. Lees, A. Lehmann, M. Sandberg, A. Hamberger, The neurotoxicity of ouabain, a sodium-potassium ATPase inhibitor, in the rat hippocampus, Neurosci. Lett. 120 (2) (1990) 159–162.

[34] D.M. Townsend, K.D. Tew, H. Tapiero, The importance of glutathione in human disease, Biomed. Pharmacother. 57 (3–4) (2003) 145–155.

[35] H.J. Forman, H. Zhang, Targeting oxidative stress in disease: promise and limitations of antioxidant therapy, Nat. Rev. Drug. Discov. 20 (9) (2021) 689–709.

[36] R. Gozzelino, V. Jeney, M.P. Soares, Mechanisms of cell protection by heme oxygenase-1, Annu. Rev. Pharmacol. Toxicol. 50 (2010) 323–354.

[37] K.D. Poss, S. Tonegawa, Reduced stress defense in heme oxygenase 1-deficient cells, Proc. Natl. Acad. Sci. USA 94 (20) (1997) 10925–10930.

[38] A.C. Morris, H.K. Hagler, J.T. Willerson, L.M. Buja, Relationship between calcium loading and impaired energy metabolism during Na+, K+ pump inhibition and metabolic inhibition in cultured neonatal rat cardiac myocytes, J. Clin. Invest. 83 (6) (1989) 1876–1887.

[39] L. de Sá Lima, E.M. Kawamoto, C.D. Munhoz, P.F. Kinoshita, A.M. Orellana, R. Curi, L.V. Rossoni, M.C. Avellar, C. Scavone, Ouabain activates NFκB through an NMDA signaling pathway in cultured cerebellar cells, Neuropharmacology 73 (2013) 327–336, https://doi.org/10.1016/j.neuropharm.2013.06.006.

[40] Y. Lavrovsky, M.L. Schwartzman, R.D. Levere, A. Kappas, N.G. Abraham, Identification of binding sites for transcription factors NF-kappa B and AP-2 in the promoter region of the human heme oxygenase 1 gene, Proc. Natl. Acad. Sci. USA 91 (13) (1994) 5987–5991.

[41] C.H. Song, N. Kim, R. Hee Nam, S. In Choi, J. Hee Son, J. Eun Yu, E. Shin, H.N. Lee, D.H. Kim, Y.J. Surh, 17beta-Estradiol strongly inhibits azoxymethane/dextran sulfate sodium-induced colorectal cancer development in Nrf2 knockout male mice, Biochem. Pharmacol. 182 (2020), 114279.

[42] W.K. Cavenee, T.P. Dryja, R.A. Phillips, W.F. Benedict, R. Godbout, B.L. Gallie, A. L. Murphree, L.C. Strong, R.L. White, Expression of recessive alleles by chromosomal mechanisms in retinoblastoma, Nature 305 (5937) (1983) 779–784.

[43] C.A. Nichols, W.J. Gibson, M.S. Brown, J.A. Kosmicki, J.P. Busanovich, H. Wei, L. M. Urbanski, N. Curimjee, A.C. Berger, G.F. Gao, A.D. Cherniack, S. Dhe-Paganon, B.R. Paolella, R. Beroukhim, Loss of heterozygosity of essential genes represents a widespread class of potential cancer vulnerabilities, Nat. Commun. 11 (1) (2020) 2517.

[44] K. Alevizopoulos, T. Calogeropoulou, F. Lang, C. Stournaras, Na+/K+ ATPase inhibitors in cancer, Curr. Drug. Targets 15 (10) (2014) 988–1000.

[45] K. Dimas, N. Papadopoulou, C. Baskakis, K.C. Prousis, M. Tsakos, S. Alkahtani, S. Honisch, F. Lang, T. Calogeropoulou, K. Alevizopoulos, C. Stournaras, Steroidal cardiac Na+/K+ ATPase inhibitors exhibit strong anti-cancer potential in vitro and in prostate and lung cancer xenografts in vivo, Anticancer. Agents. Med. Chem. 14 (5) (2014) 762–770.

[46] T. Hemachand, C. Shaha, Functional role of sperm surface glutathione S-transferases and extracellular glutathione in the haploid spermatozoa under oxidative stress, FEBS Lett. 538 (1–3) (2003) 14–18.

[47] M.J. Morgan, Z.G. Liu, Crosstalk of reactive oxygen species and NF-kappaB signaling, Cell. Res. 21 (1) (2011) 103–115.

[48] J.D. Hayes, A.T. Dinkova-Kostova, K.D. Tew, Oxidative Stress in Cancer, Cancer Cell 38 (2) (2020) 167–197.

[49] O.J. Ziff, D. Kotecha, Digoxin: The good and the bad, Trends. Cardiovasc. Med. 26 (7) (2016) 585–595.

[50] J. Lin, T. Zhan, D. Duffy, J. Hoffman-Censits, D. Kilpatrick, E.J. Trabulsi, C. D. Lallas, I. Chervoneva, K. Limentani, B. Kennedy, S. Kessler, L. Gomella, E. S. Antonarakis, M.A. Carducci, T. Force, W.K. Kelly, A pilot phase II Study of digoxin in patients with recurrent prostate cancer as evident by a rising PSA, Am. J. Cancer. Ther. Pharmacol. 2 (1) (2014) 21–32.

[51] H. Sakai, T. Suzuki, M. Maeda, Y. Takahashi, N. Horikawa, T. Minamimura, K. Tsukada, N. Takeguchi, Up-regulation of Na(+), K(+)-ATPase alpha 3-isoform and down-regulation of the alpha1-isoform in human colorectal cancer, FEBS Lett. 563 (1–3) (2004) 151–154.

[52] M. Baker Bechmann, D. Rotoli, M. Morales, C. Maeso Mdel, P. Garcia Mdel, J. Avila, A. Mobasheri, P. Martin-Vasallo, Na,K-ATPase Isozymes in Colorectal Cancer and Liver Metastases, Front. Physiol. 7 (2016) 9.

[53] G. Crambert, U. Hasler, A.T. Beggah, C. Yu, N.N. Modyanov, J.D. Horisberger, L. Lelievre, K. Geering, Transport and pharmacological properties of nine different human Na, K-ATPase. isozymes, J. Biol. Chem. 275 (3) (2000) 1976–1986.

[54] A. Talevi, Multi-target pharmacology: possibilities and limitations of the "skeleton key approach" from a medicinal chemist perspective, Front. Pharmacol. 6 (2015) 205.

[55] M. Matejcic, M. Vogelsang, Y. Wang, M. Iqbal Parker, NAT1 and NAT2 genetic polymorphisms and environmental exposure as risk factors for oesophageal squamous cell carcinoma: a case-control study, BMC Cancer 15 (2015) 150.

[56] X.G. Ke, Y.Y. Xiong, B. Yu, C. Yuan, P.Y. Chen, Y.F. Yang, H.Z. Wu, Mollugin induced oxidative DNA damage via up-regulating ROS that caused cell cycle arrest in hepatoma cells, Chem. Biol. Interact. 353 (2022), 109805.

[57] C.A. Smith, E.J. Want, G. O'Maille, R. Abagyan, G. Siuzdak, XCMS: processing mass spectrometry data for metabolite profiling using nonlinear peak alignment, matching, and identification, Anal. Chem. 78 (3) (2006) 779–787.

[58] S. Li, Y. Park, S. Duraisingham, F.H. Strobel, N. Khan, Q.A. Soltow, D.P. Jones, B. Pulendran, Predicting network activity from high throughput metabolomics, PLoS Comput. Biol. 9 (7) (2013), e1003123.

[59] A.M. Orellana, J.A. Leite, P.F. Kinoshita, A.R. Vasconcelos, D.Z. Andreotti, L. de Sá Lima, G.F. Xavier, E.M. Kawamoto, C. Scavone, Ouabain increases neuronal branching in hippocampus and improves spatial memory, Neuropharmacology 15 (2018) 140–274, https://doi.org/10.1016/j.neuropharm.2018.08.008.